The Effect of Aluminum Content on the Corrosion Behavior of Fe-Al Alloys in Reducing Environments at 700 °C

S.W. BANOVIC, J.N. DuPONT, and A.R. MARDER

The high-temperature corrosion behavior of monolithic Fe-Al alloys, with 0 to 20 wt pct Al, was investigated at 700 °C in a reducing atmosphere ($p(S_2) = 10^{-4}$ atm, $p(O_2) = 10^{-25}$ atm) for up to 100 hours. Postexposure characterization of the corrosion reaction products consisted of surface and cross-sectional microscopy, in combination with energy dispersive spectroscopy, electron probe microanalysis, and quantitative image analysis. From the kinetic data, three stages of corrosion behavior (*i.e.*, inhibition, breakdown, and steady state) were found with the observance and/or duration of each stage directly related to the aluminum content of the alloy. The first stage, labeled the inhibition stage, was characterized by low weight gains and the absence of rapid degradation of the alloy. Typically observed for compositions with 10 to 20 wt pct Al, protection was afforded due to the development of a thin, continuous alumina scale. For alloys with 7.5 wt pct Al, the ability to maintain the initially formed alumina scale was not observed, resulting in the breakdown stage. Localized corrosion product nodules, containing iron sulfide ($Fe_{1-x}S$) and the spinel-type tau phase ($FeAl_2S_4$), developed through the alumina scale due to sulfur short-circuit diffusion. These growths were accompanied by relatively high corrosion rates. Further decreasing the aluminum content to 5 wt pct and below lead to the formation of a continuous sulfide scale whose growth was controlled by iron and sulfur diffusion through the previously formed product. The alloy wastage rates in the steady-state stage were relatively high when compared to the previous two regions.

I. INTRODUCTION

WELD overlay coatings are typically being applied in order to protect existing waterwall panels of utility boilers from accelerated sulfidation attack. By depositing an alloy that offers better corrosion resistance than the underlying tube material, typically a low alloy steel, the wastage rates can be reduced. While Ni-base and stainless steel compositions are presently providing protection, they are expensive and susceptible to failure *via* corrosion fatigue due to microsegregation, which occurs upon solidification.[1] Another material system presently under consideration for use as a coating in the oxidation/sulfidation environments is iron-aluminum. These alloys are relatively inexpensive and do not exhibit microsegregation.[2] In addition, studies[3–12] in very aggressive environments (gas compositions containing upwards of 3500 ppm H_2S and temperatures above 700 °C) have shown that alloys with more than 10 wt pct Al possess excellent sulfidation resistance. This decrease in the corrosion rates was attributed to a protective alumina (Al_2O_3) scale that was able to form in the mixed environments (highly sulfidizing with low partial pressures of oxygen). However, even with superior sulfidation resistance, Fe-Al alloys are not presently applied as coatings due to a weldability problem. Above 10 wt pct Al, these alloys readily crack during welding, due to hydrogen cracking susceptibility, when deposited without extensive preheat and postweld heat treatments.[2] The intensity of the problem has been found to increase with an increase in the aluminum content of the alloy.[2,13–15] In addition to the weldability problem, detailed corrosion studies to assess the performance of these alloys in environments representative of gas conditions found for boilers with low NO_x burners is limited in the open literature,[6,16,17] as these conditions are less aggressive than those previously mentioned. Therefore, the objective of this research was to systematically study the effect of aluminum content on the corrosion behavior of low aluminum Fe-Al alloys in moderately reducing environments at 700 °C.

II. EXPERIMENTAL PROCEDURE

The Fe-Al alloys used during this research were produced at Oak Ridge National Laboratory (Oak Ridge, TN) by arc melting high purity Fe (99.99 pct) and Al (99.99 pct) under argon and drop casting into a water-cooled copper mold. Substrates, with dimensions of 1 cm by 1 cm by 2 mm, were sectioned from the bulk using a high speed diamond saw, followed by grinding of the surface to 600 grit. Specimens were prepared immediately before insertion into the balance with prior steps of ultrasonic cleaning in soapy water and methanol.

A Netzsch STA 409 (Paoli, PA) high-temperature thermogravimetric balance was used to measure weight gain as a function of time, with the gas composition chosen to produce a highly reducing environment that was indicative of low NO_x gas conditions typically found in utility boilers.[18,19,20] Table I shows the gas composition, as reported by Scott Specialty Gases (Plumsteadville, PA), and the corresponding partial pressure of oxygen [$p(O_2)$] and sulfur [$p(S_2)$] values at exposure temperature. The $p(O_2)$ was determined using a solid-state oxygen detector, and the $p(S_2)$ was calculated using the SolGasMix program.[21] At test temperature, the location of the testing environment was found to lie in a region of aluminum oxide and iron sulfide, X in Figure 1,

S.W. BANOVIC, Research Associate, J.N. DuPONT, Assistant Professor, and A.R. MARDER, Professor, are with the Department of Materials Science and Engineering, Lehigh University, Bethlehem, PA 18015.

Manuscript submitted January 18, 2000.

Table I. Corrosion Gas Composition (by Volume Percent) and Corresponding Partial Pressures of Oxygen (Measured) and Sulfur (Calculated) at Exposure Temperature

Gas Composition	Temperature	$p(O_2)$	$p(S_2)$
1.0 pct H_2S - 0.1 pct H_2 - 98.9 pct Ar - 5 ppm O_2	700 °C	3.4×10^{-25} atm	5.4×10^{-4} atm

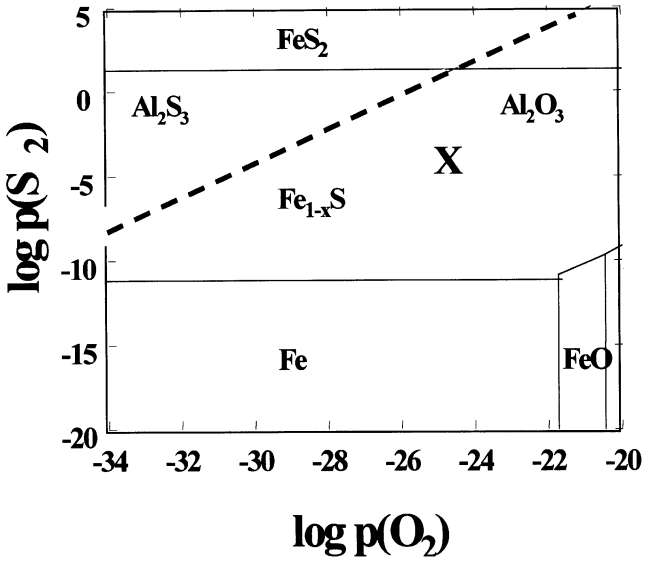

Fig. 1—Superimposed thermostability diagrams for Fe and Al at 700 °C calculated using Ref. 21. The solid lines represent the coexistence lines between the iron base phases, while the dashed line is for the aluminum containing phases. The exposure atmosphere for the reducing conditions is denoted by X.

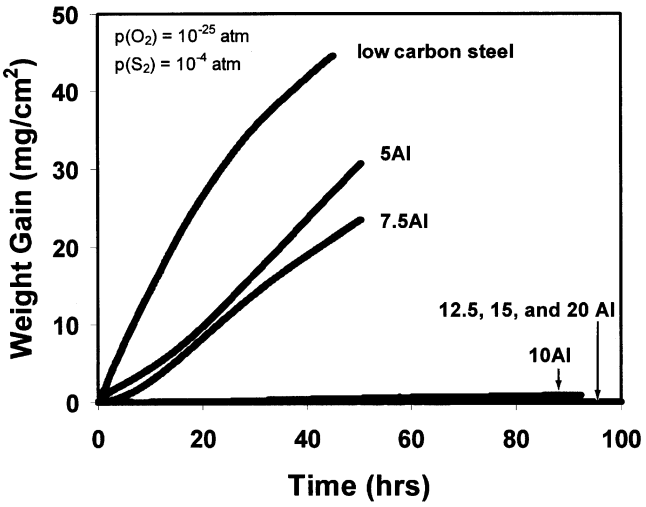

Fig. 2—Weight gain *vs* time for the longest exposure time for each alloy at 700 °C. As aluminum content increased, the weight gains were found to decrease.

according to superimposed thermostability diagrams for iron and aluminum. After purging for 2 hours at room temperature in the exposure gas, samples were heated at a rate of 50 °C per minute and isothermally held at 700 °C for various times (1, 5, 15, 25, 50, and/or 100 hours).

Postexposure characterization of the corroded surfaces was conducted using a JEOL* 6300F scanning electron microscope (SEM) with an Oxford (Link) energy dispersive spectroscopy (EDS) system capable of detecting light elements, particularly oxygen. Polished cross sections were obtained by mounting in cold setting epoxy with subsequent grinding procedures to 1200 grit with silicon carbide papers. A final polishing step was conducted using 1 μm diamond paste on a low nap cloth. Further polishing with any type of colloidal alumina or silica was avoided in order to minimize any possibilities of contamination or pullout of the scale. The use of 200 proof, dehydrated ethanol was used for both lubrication and cleansing solution during preparation in order to avoid degradation of the corrosion products from water.[22] Cross-sectional scale thicknesses were measured on secondary electron (SE) micrographs using a Donsanto digitizing pad interfaced with a Nikon Optiphot microscope. A minimum of 20 measurements were taken per layer per sample on various planes. Quantitative chemical information was obtained using a JEOL 733 electron probe microanalyzer (EPMA) equipped with wavelength dispersive spectrometers (WDS). The accelerating voltage and probe current were 20 kV and 50 nA, respectively. The K_a X-ray lines were analyzed and counts converted to wt pct using a $\varphi(\rho z)$ correction scheme.[23]

A fracturing technique using liquid nitrogen was also employed to view the scales in cross section. By notching the back side, approximately 4/5 of the thickness of the substrate, with a low speed diamond saw and submersing the specimen for a minimum of 3 minutes in liquid nitrogen, the samples easily broke. Cross-sectional micrographs of these samples were also taken using the JEOL 6300F.

*JEOL is a trademark of Japan Electron Optics Ltd., Tokyo.

III. RESULTS

A. *Corrosion Kinetics*

Figure 2 displays the kinetic results obtained at the temperature for the longest exposure time for each alloy (either 50 or 100 hours). The trend observed was decreasing weight changes with increasing aluminum content. Once above 7.5 wt pct Al, the increase in weight was relatively small. In all cases, shorter time exposures (1, 5, 15, and 25 hours) followed their respective weight gain data curves for the longer times with good reproducibility.

B. *Corrosion Morphologies*

The low-carbon steel sample was found to have a bilayered scale, as shown in Figure 3. The EPMA data indicated that both layers were iron sulfide ($Fe_{1-x}S$), with the outer scale being relatively dense with a columnar appearance, and the inner as fine grained and porous. Separation between these two can be observed indicating poor adhesion between the different morphologies. Similarly, the 5 wt pct Al alloy

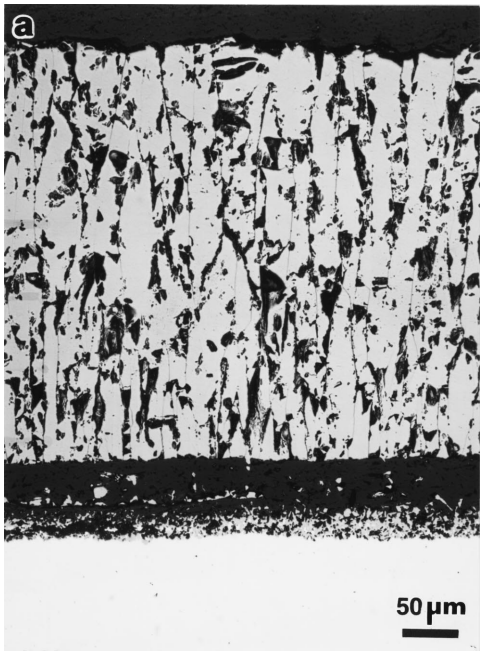

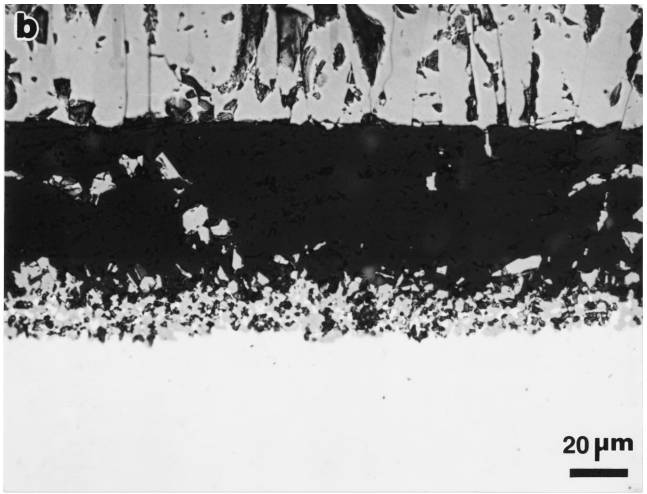

Fig. 3—Light optical micrographs showing the polished cross section of the low-carbon steel sample after 50 h of exposure at 700 °C. (*a*) The bilayered, iron sulfide scale with outer columnar grains and inner fine grained layer. (*b*) Inner scale with separation between layers.

grew a continuous surface scale that was also bilayered (Figure 4). The EPMA analysis (Table II) showed that the outer scale consisted of irregularly shaped iron sulfide ($Fe_{1-x}S$) plates, with approximately 1 wt pct Al in solution near their base at the inner scale–outer scale interface. The inner scale was found to be composed of tau plates ($FeAl_2S_4$, a spinel-type compound, dark in Figures 4(b) and (c)) and iron sulfide particles (light particles in Figures 4(b) and (c)). A fair amount of porosity was also noted (black in Figure 4(c)). The EPMA traces into the substrate did not reveal depletion of either metallic element (Fe, Al) or the ingress of sulfur into the alloy, within the resolution limits of the equipment (~1 μm). Figure 5 shows the variation of scale thickness with time for both alloys. Time rate growth constants (n) were calculated by fitting the data to a power law relationship:

$$x = kt^n + C \qquad [1]$$

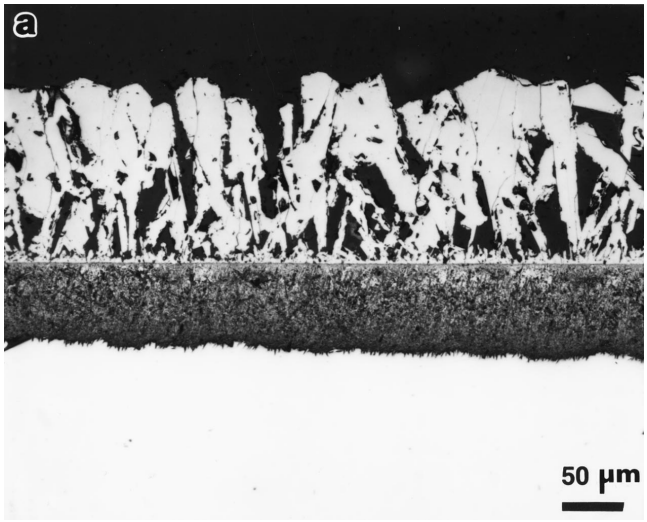

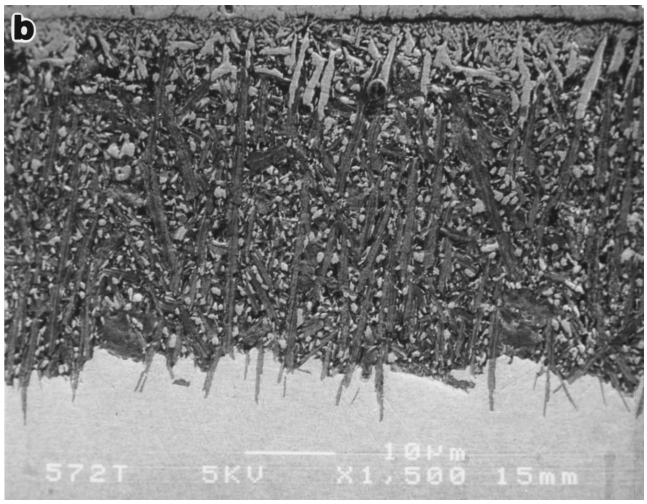

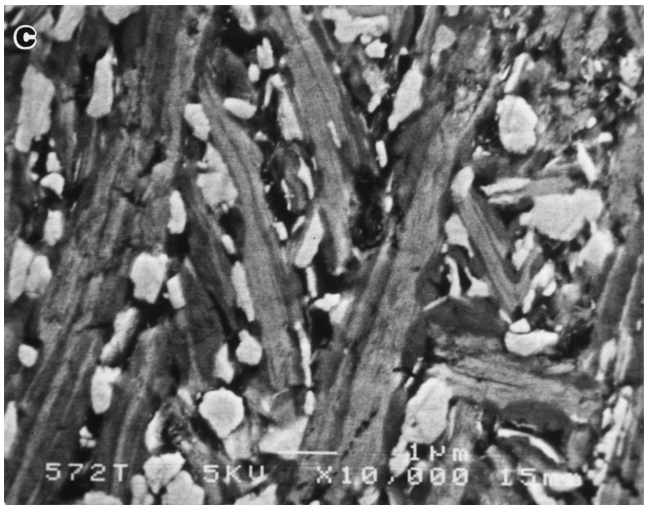

Fig. 4—Polished cross section of the Fe-5 wt pct Al sample after 50 h of exposure at 700 °C. (*a*) Light optical micrograph of the bilayered scale showing the outer iron sulfide grains and inner layer. (*b*) and (*c*) SE micrographs of the inner scale containing iron sulfide (light colored particles), tau plates (dark), and porosity (black regions).

where x is the scale thickness (or weight gain per surface area), t is time, and k and C are constants. By taking the log of both sides,

Table II. Representative EPMA Data for Thick Sulfide Phases Taken from the Fe-5 Wt Pct Al Alloy

Scale Feature	Fe	Al	S	Phase(s)
Outer columnar scale	61.7 ± 0.5	0.0	37.7 ± 0.3	$Fe_{1-x}S$
Base of outer scale	61.7 ± 0.5	0.9 ± 0.2	37.6 ± 0.4	$Fe_{1-x}S$ with Al
Scan of inner layer	45.1 ± 0.3	8.3 ± 0.5	43.3 ± 0.7	tau + $Fe_{1-x}S$
Dark, inner layer plate	24.0 ± 0.8	20.7 ± 0.3	52.8 ± 1.0	tau

Table III. Calculated Time Rate Growth Constants (*n*) for Various Microstructural Features of Selected Samples

Alloy	Scale Measurement	*n* Value	Fit (R^2)
Low-carbon steel	total iron sulfide scale	0.51	0.99
Fe-5 wt pct Al	total scale growth	0.68	0.99
Fe-5 wt pct Al	outer iron sulfide scale	0.63	0.98
Fe-5 wt pct Al	inner mixed sulfide scale	0.61	0.99
Fe-7.5 wt pct Al	nodule diameter, lateral growth	0.95	0.99
Fe-7.5 wt pct Al	inner scale growth, perpendicular to surface	0.63	0.99

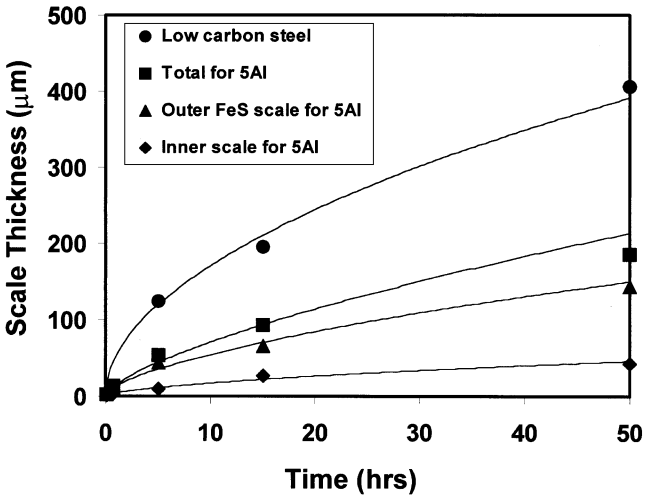

Fig. 5—Cross-sectional scale thickness as a function of time for the low-carbon steel sample and the Fe-5 wt pct Al alloy.

$$\log(x) = n * \log(t) + C' \quad [2]$$

the *n* value can be found. Values for which *n* equals 1, 0.5, or 0.3 follow linear, parabolic, or cubic growth rates, respectively. Table III displays these calculated values.

Samples with 10 to 20 wt pct Al had the appearance of either a tan, blue, or purple color upon removal from the specimen chamber. The SE micrographs of the surfaces revealed coverage by small platelet growths (Figure 6) out of a granular scale, and the lack of thick scale development as observed for the previous samples. The small size of the platelets inhibited direct chemical analysis of individual particles, however, a cluster of platelets were analyzed with EDS indicating the presence of iron, aluminum, and sulfur, which would be consistent with a sulfide phase. As can be seen in Figure 6, increasing the aluminum content of the sample from 10 to 20 wt pct decreased the number and size of these features. In addition, the relative size of the platelets, in terms of diameter and length, was found to increase up

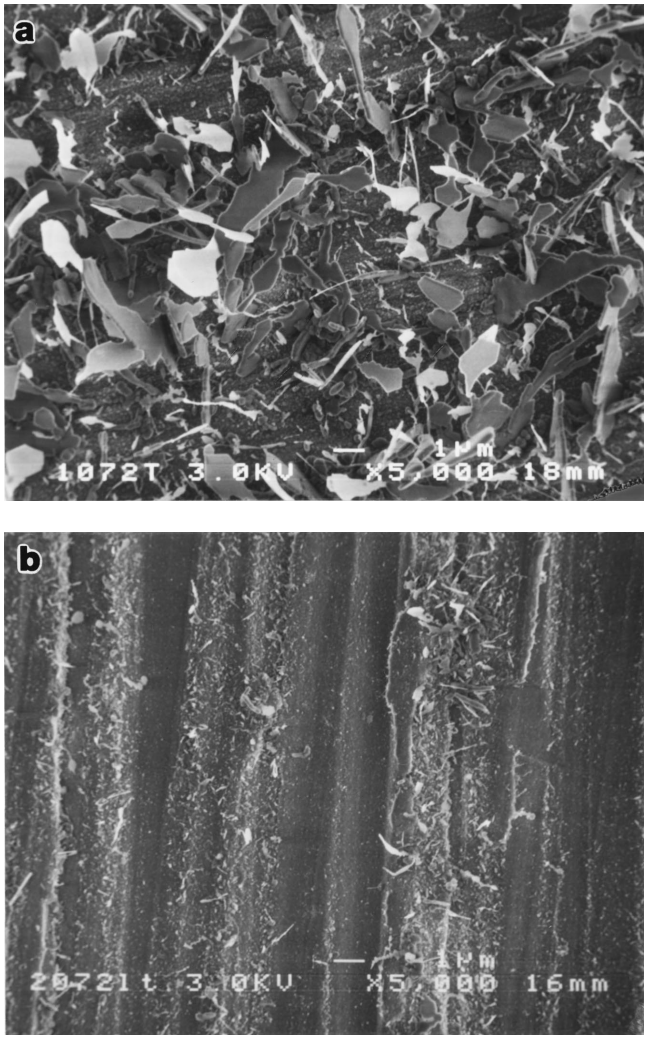

Fig. 6—Characteristic SE images of the platelets formed on the surface of high aluminum alloys. (*a*) High density of platelets found on alloys with 10 to 12.5 wt pct. (*b*) Less populated areas found on alloys with 15 to 20 wt pct. Both after 100 h of exposure al 700 °C.

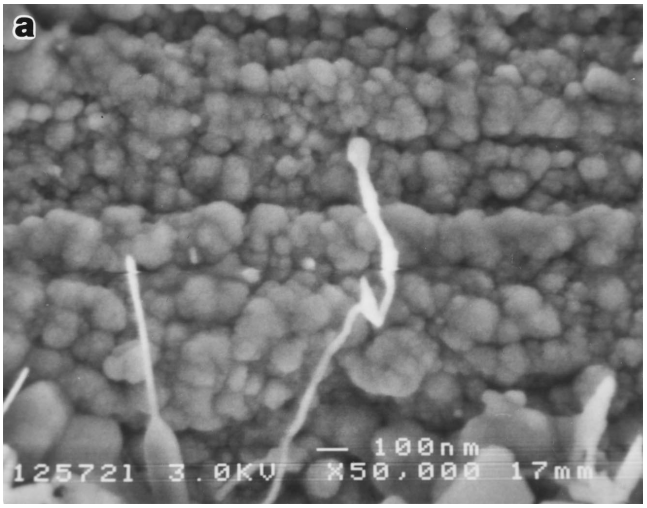

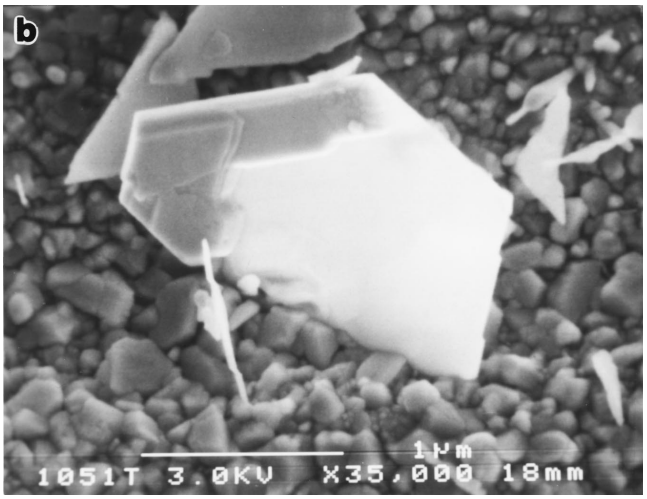

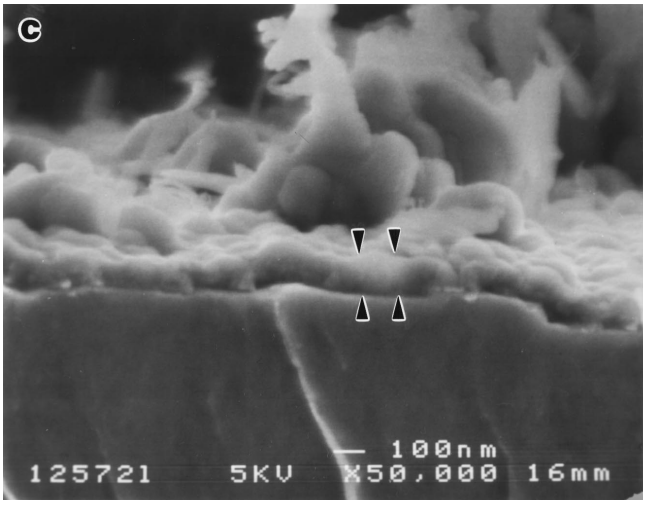

Fig. 7—Characteristic SE image of the granular background scale formed on high aluminum alloys at 700 °C. (*a*) Surface after 50 h, (*b*) growth of sulfide platelet from between the grains of the scale after 100 h, and (*c*) fractured cross section after 50 h with arrows indicating thickness. Sample shown is Fe-10 wt pct Al.

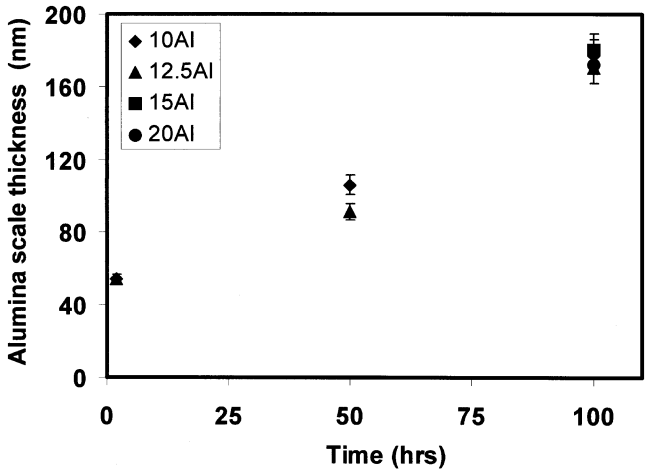

Fig. 8—Plot of cross-sectional alumina scale thickness formed on high-aluminum alloys as a function of time.

to 50 hours, where after they remained relatively constant with further exposure to 100 hours. Analysis of the granular scale in the background (Figure 7) by EDS indicated high counts of Al and O with low counts of Fe and S. Growth of the sulfide platelets appear to grow from between the grains of the granular scale (Figure 7(b)). As shown by fractured cross-sectional micrographs in these areas (Figure 7(c)), the scale appeared to be uniform with its thickness increasing with time (Figure 8). However, changes in aluminum alloy content, from 10 to 20 wt pct, did not lead to significant differences in scale morphology or thickness. On occasion, small nodule growths were observed to form at the corners or edges of the 10 and 12.5 wt pct Al specimens (Figure 9(b)) but were never encountered on the flat faces of the sample.

Aluminum contents of 7.5 wt pct developed localized sulfide growths that were found randomly dispersed across the surfaces, as shown in Figure 10. The nodules had a similar appearance regardless of the exposure time. For extended exposures, above 15 hours, some coalescence of the nodules was observed with their lateral growth linearly related to time (Figure 11(a)). The time rate growth constant can be found in Table III. It did not appear that the substrate grain boundaries played a major role in the location of the nodules as they were well dispersed across the sample face. In the nodule-free areas, a granular surface scale, similar to the one found on the higher aluminum alloys, was present. Cross-sectional analysis (Figure 12) showed that the nodules consisted of similar phases as seen in the thick scale growths. The overall appearance had a lenticular shape with further analysis revealing the outer scale of thick iron sulfide ($Fe_{1-x}S$) plates with various growth directions (Figure 12(a)). The inner scale was also composed of tau plates and iron sulfide particles, similar compositions to those found in Table II, that developed normal to the surface with a near parabolic relationship with time (Figure 11(b) with the *n* value located in Table III). Higher magnification at the inner scale–outer scale interface revealed the remnants of a thin surface scale (Figure 12(b)). This was observed to span the entire length of the nodule cross section. In the substrate directly below the nodules, EPMA analysis did not indicate the presence of sulfur or the depletion of either metallic element. The same can be said for the alloy located below the thin granular scale.

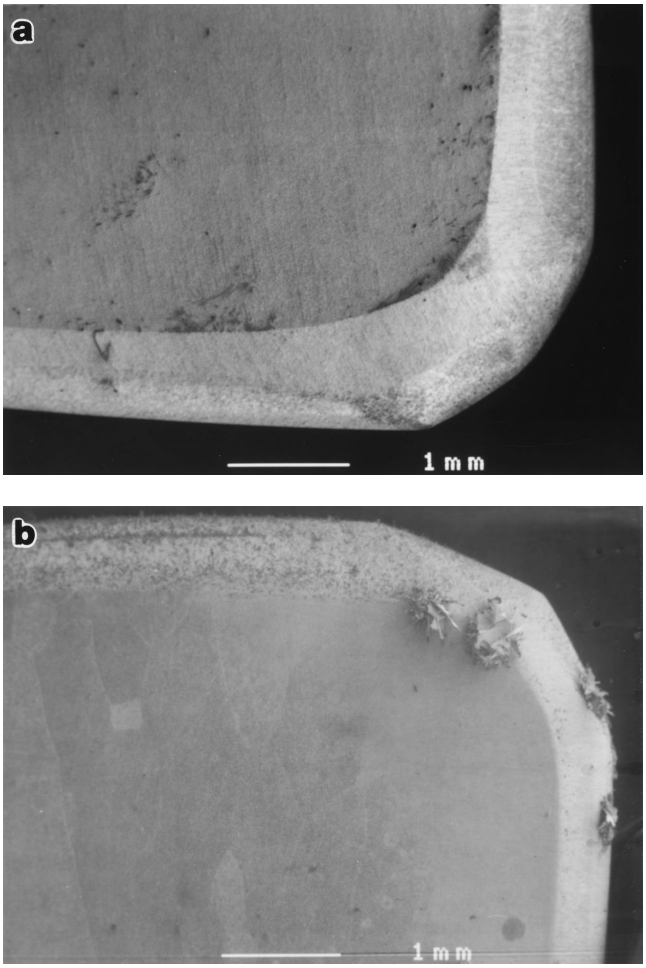

Fig. 9—Low-magnification SE image of the Fe-10 wt pct Al sample exposed for (*a*) 2 h and (*b*) 100 h at 700 °C. Formation of small nodular growths of corrosion product can be observed at the corners and edges of the sample on the latter micrograph.

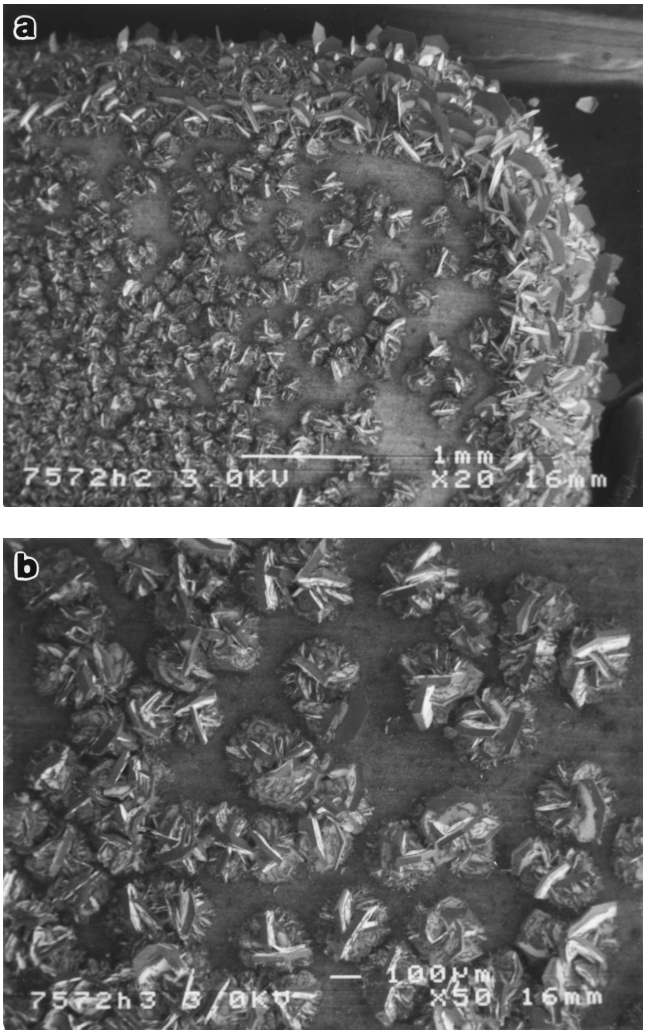

Fig. 10—(*a*) and (*b*) SE images of the surface of the Fe-7.5 wt pct Al sample exposed for 20 h showing the localized sulfide growths in the form of nodules.

IV. DISCUSSION

A. *General Corrosion Behavior*

The corrosion behavior of Fe-Al alloys in the oxidizing/sulfidizing environment was found to be directly dependent upon the aluminum content of the alloy, which influenced the type and morphology of corrosion product that formed during high-temperature exposure. These products were typically in the form of a surface scale, or scales, that developed with time. Depending on which reaction product developed, the alloys were found to exhibit one, if not more, of three stages of corrosion behavior: inhibition, breakdown, and steady state. Schematic representations of these regions are found by plotting the weight gain data on logarithmic axes (Figure 13(a)) with the development of the scale(s) observed in Figure 14.

The inhibition stage was typified by initial growth of a thin, passive surface scale that suppressed excessive degradation of the substrate (Figure 14(a)) and resulted in low weight gains due to its ability to impede the formation of fast-growing corrosion products incorporating sulfur. These low weight gains were observed due to slow diffusion of both cation and anion species through the continuous layer. However, this stage was not always found to last the duration of the test. Mechanical failure of the scale (Figure 14(b)), with the inability to re-establish itself (depending upon aluminum content of the alloy), led to the growth of nonprotective sulfide phases due to short circuiting of the passive layer by sulfur, as shown in Figure 14(c). Extremely rapid weight gains (Figure 13(a)) were often associated with this stage as continued growth did not solely depend upon diffusion of the specie through the previously formed product, but in addition, the further mechanical deterioration of the passive layer. This resulted in faster growth along a lateral direction with respect to the substrate surface instead of perpendicular to it. With time, the nodules were observed to spread and coalesce to form a continuous surface scale of sulfides. These continuous sulfide scales were also formed on the low-aluminum alloys from the onset of exposure (Figure 14(d)). After initially high corrosion rates, a steady-state regime of weight gain was encountered (Figure 13(a)) as sustained growth of the thick scale occurred *via* a diffusion mechanism. However, the morphology of these resulting multilayered, multiphase scales did not allow for direct quantification of the diffusing specie through analysis of the continuous weight gain data. The following sections will

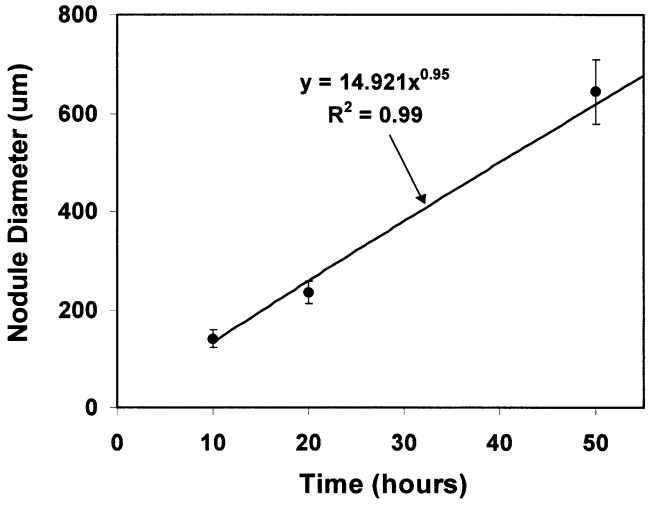

(*a*)

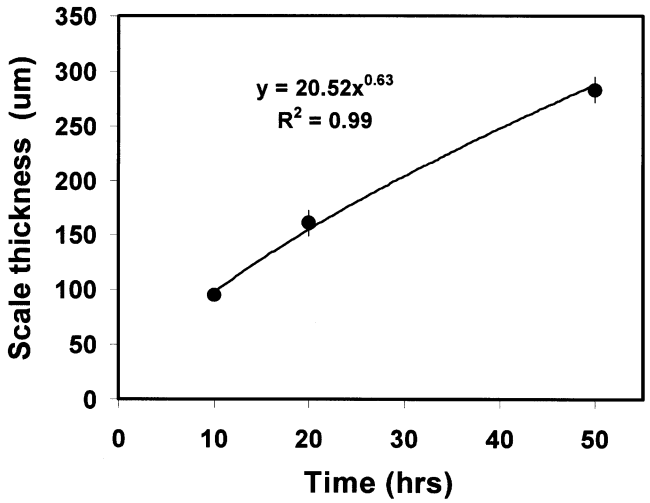

(*b*)

Fig. 11—(*a*) Plot of lateral growth of sulfide nodules parallel to the surface as a function of time, and (*b*) plot of inner scale development perpendicular to the surface *vs* time for the Fe-7.5 wt pct Al samples.

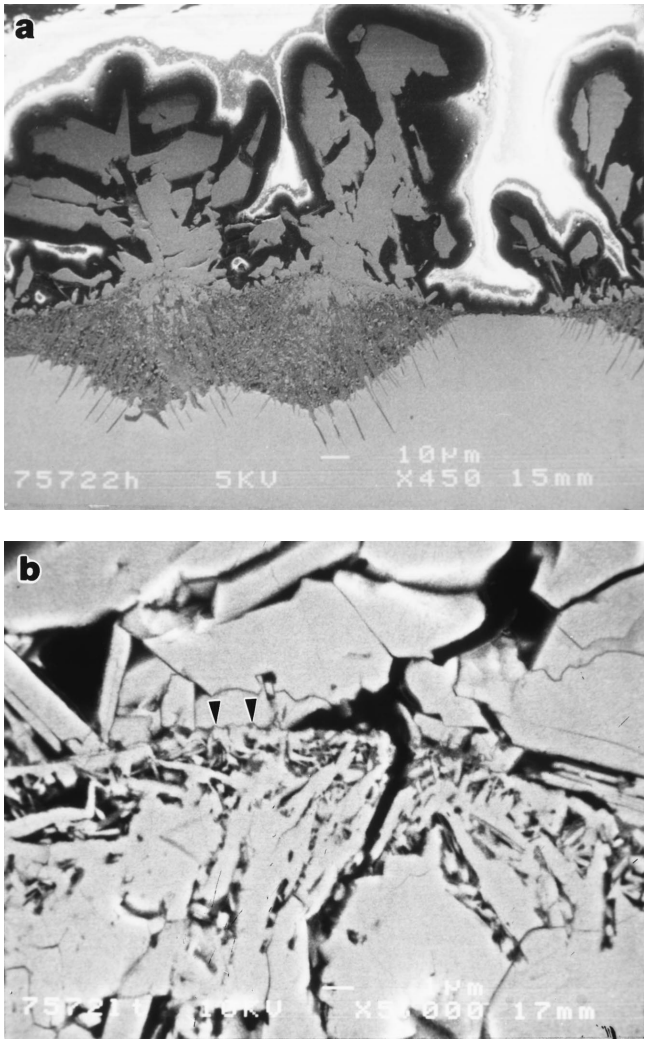

Fig. 12—Polished cross-sectional SE micrographs of the Fe-7.5 wt pct Al sample showing (*a*) the lenticular nature of the nodule and (*b*) the remnants of an original surface scale between the outer iron sulfide scale and inner mixed sulfide layer as indicated by arrows.

further discuss the three stages of corrosion behavior in more detail with respect to the aluminum content of the alloy.

1. *Inhibition stage*

Additions of aluminum were found to decrease the corrosion rates by promoting the formation of a slower growing, surface reaction product on the alloy during exposure. This was generally observed from the weight gain data obtained during corrosion testing with alloys richer in aluminum having ideal corrosion protection. The protective surface scale was composed of tightly packed, equiaxed grains containing high amounts of aluminum and oxygen (Figure 7(a)). While definitive identification of the scale could not be made, enough evidence suggests that it is an aluminum oxide, probably gamma alumina, in terms of the EDS analysis, color,[24] temperature regime in which it has formed,[25] and its protective nature (in terms of weight gain, (Figure 2) and thickness (Figures 7(c) and 8)). In addition, DeVan[3] also observed protective behavior from development of a gamma alumina scale in similar mixed environments on iron aluminide compositions. The alumina scale formed due to preferential oxidation of the aluminum on the alloy surface, and the results from this study, in terms of weight gain, indicated that its formation was promoted through increasing the aluminum content of the alloy.

In order for protective behavior to occur, a continuous scale of alumina must form upon initial exposure. According to superimposed thermostability diagrams for iron and aluminum, the location of the testing environment was found to lie in a region of alumina and iron sulfide (Figure 1). These are the two phases that will be stable on the Fe-Al alloy surface at initial exposure with respect to the given atmosphere and temperature. During the very early stages of reaction, it is expected that both phases will nucleate on the surface due to thermodynamic considerations. Whether a continuous, protective scale will form is dependent upon the density and dispersion of its nuclei, as well as the relative diffusion rates in the alloy and scale.[26] Since the sulfide products typically grow faster due to their highly defective structures,[27] it is imperative that alumina nuclei have widespread and dense coverage of the surface to suppress growth of the nonprotective phases. This study showed that by increasing the amount of aluminum in the alloy, the probability of forming a continuous scale of alumina was improved.

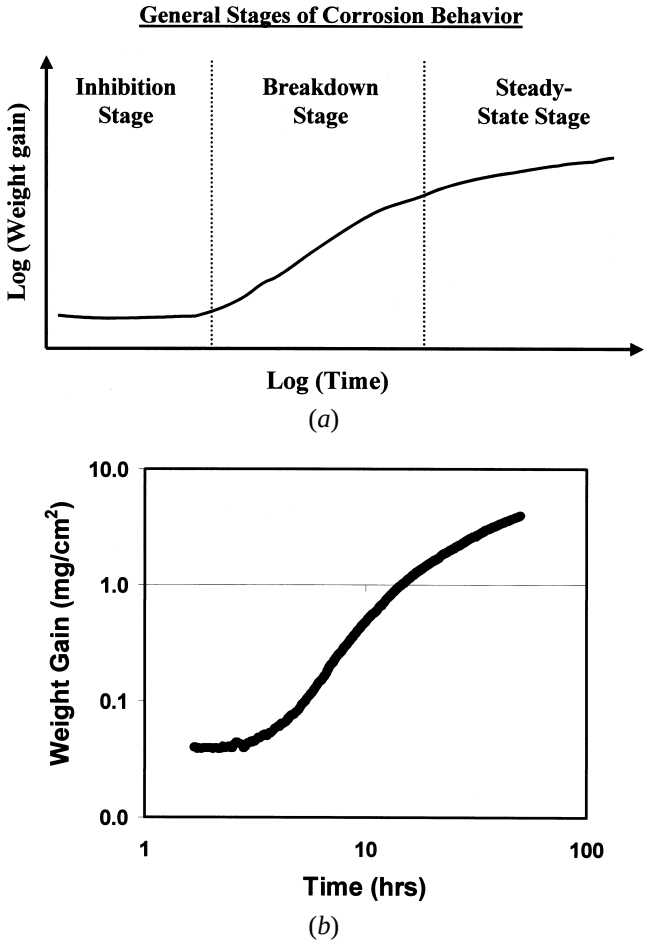

Fig. 13—(*a*) Schematic showing the three stages of corrosion behavior observed by the Fe-Al alloys. (*b*) Plot of weight gain *vs* time, on a logarithmic scale, for the Fe-10 wt pct Al sample showing the three stages of corrosion.

This may be due to the decreased distance between adjacent alumina nuclei on the surface at early times, thus, requiring less lateral growth, and concurrently less time, to obtain full surface coverage of the protective phase.

The protectiveness of the alumina scale was found to manifest itself in three ways: 1) low weight gains and corresponding scale thickness, 2) lack of sulfur ingress, and 3) slow rate of cation diffusion. While it is intuitive that a protective scale will result in lower weight gains, it is also important to note the thickness of the scale that provides protection at temperature. The alumina scales observed to grow on the high aluminum alloys at 700 °C barely attained 200 nm of growth over the 100 hour exposure period yet were able to maintain less than 0.2 mg/cm^2 in weight gain. Other crystalline phases of alumina, such as alpha, have been found to provide protection at higher temperatures (typically above 1000 °C) for intermetallic iron-aluminum compositions but have a tendency to become much thicker over time even though their weight gains are also relatively low. At exposure temperature, these scales can grow to a thickness of 8 μm within 100 hours.[28] Preferential aluminum removal through this type of thick scale growth depletes the alloy of this element at a relatively fast rate. This rate of aluminum consumption is critical when considering these alloys for industrial applications, in particular, weld overlay coatings. As previously mentioned,[2] the weldable compositions considered here have relatively low aluminum reserves to begin with ($\leq$10 wt pct Al).

The effectiveness of a coating, in terms of corrosion resistance, can be defined by the oxidation lifetime or the amount of time over which a surface scale will provide protection for the underlying substrate. This concept was studied and modeled by Quadakkers and co-workers[29,30] and recently reviewed by Tortorelli and Natesan.[12] The time frame for protection has been found to be a function of the total amount of aluminum available for reaction (at the surface and in reserve) and the rate at which it is consumed. Oxidation lifetime of an alloy ends when the aluminum content falls below a composition such that formation of the alumina scale is not possible and the development of less protective products can occur leading to breakaway corrosion. A major

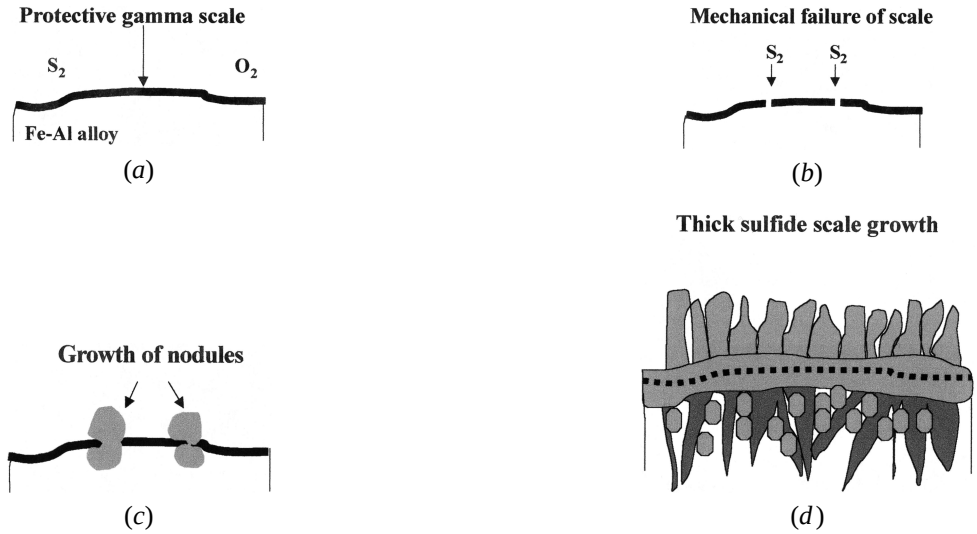

Fig. 14—Schematic showing the surface scale development in relation to the three stages of corrosion. (*a*) Initial protection by the alumina scale during the inhibition stage, (*b*) mechanical failure of the alumina scale with sulfur short circuit diffusion at the start of the breakdown stage, (*c*) nucleation and growth of the sulfide phases through the alumina scale during the breakdown stage, and (*d*) thick scale coverage by the bilayered sulfide phases.

cause leading to aluminum depletion can be through thermal cycling where repeated spallation and re-growth of the alumina scale can readily deplete the alloy of aluminum.[7,8,11]

The use of Fe-Al alloys as weld overlay coatings will automatically limit the reservoir of aluminum due to the thickness of the deposited overlay, typically 1 to 2 mm. Therefore, it is natural to conclude that increasing the amount of aluminum in the deposit will further increase the oxidation lifetime of the coating. However, it has been shown that a limit (approximately 10 wt pct Al) is imposed on the system in order to produce sound coatings depositing under conditions typically utilized in practice.[2] Aluminum contents above this value have been found to be susceptible to cold cracking subsequent to welding, which would allow for direct access of the corroding specie to the less corrosion resistant substrate, typically a low alloy steel. Therefore, without the option of increasing the aluminum content, the other alternative to increasing the oxidation lifetime of weldable compositions is by reducing the rate at which aluminum is consumed. In this study, it was shown through the thickness (thinness) of the scale that the rate of aluminum consumption at this test temperature was very low, barely 200 nm after 100 hours of exposure (Figure 8). In addition, this low thickness may be beneficial in that large growth stresses, which could enhance spallation of the scale, may not develop. While neither thermal cycling of the specimens nor stress measurements of the scale were conducted during this phase of the work, at no time was the alumina scale ever observed to crack, spall, or flake off, even after fracturing in liquid nitrogen temperatures. This suggests a somewhat adherent scale. Therefore, the "thinness" of the scale over extended periods of time, combined with the lack of spallation, results in a very low rate of aluminum consumption and may suggest a potentially long oxidation lifetime for the weldable alloys at this temperature.

While the alumina scale was able to maintain low weight gains for extended periods of time, it was also protective in the fact that internal sulfidation of the alloy was not encountered. Microprobe traces near the alloy-scale interface did not detect an increase in sulfur when compared to far distances into the substrate. This suggests that the scale was relatively impervious to inward diffusion of the anion and may be related to the fact that gamma alumina primarily grows *via* an outward cation diffusion mechanism.[25,31] It will be shown subsequently that sulfur penetration can be disastrous to the protective nature of the scale due to the formation of sulfide phases beneath its surface, which can lead to mechanical degradation of the passive layer.

While the alumina scale was impermeable to sulfur, the diffusion of iron outward was readily observed on the surface in the form of the small sulfide platelets (Figure 6). These platelets appear to grow from the alumina grain boundaries (Figure 7(b)), which suggests a weakness in the scale. However, the sulfide platelets tend to stop growing, in terms of thickness and/or number, on the high aluminum samples after a certain time (roughly 50 hours) implying that the scale may have been able to inhibit iron diffusion outward at longer exposures. Concerning this type of outward iron diffusion, the aluminum content of the alloy was found to play a major role in the number and size of the plates observed. The 15 and 20 wt pct Al samples were found to have very limited growth of the sulfides across their surfaces (Figure 6(b)), whereas the lower aluminum content alloys have thicker and more dense coverage of the platelets (Figure 6(a)). However, the development of these platelets did not appear deleterious to the protectiveness of the scale, as overall weight gain for all alloys above 7.5 wt pct Al was relatively low (Figure 2).

2. *Breakdown stage*

The ability of the alumina scale to maintain the overall passive nature was found to decrease as the aluminum content of the alloy decreased. This was primarily due to the mechanical breakdown of the alumina scale in combination with the inability to re-establish itself. Ensuing growths typically took the form of localized sulfide nodules. The shape of the continuous weight-gain data curves (Figure 13) and the remnants of the initial surface scale between the two interfacial layers (Figure 12(b)) help to prove this short-circuit diffusion mechanism. This loss of protection was most notable in the 10 wt pct Al sample exposed for 50 hours (Figure 13(b)). As shown, low weight gains occurred for the first 2 hours as a continuous and protective scale initially formed to inhibit nodular sulfide growths (Figure 9(a)). However, with time, mechanical failure in the alumina scale lead to the development of a few sulfide nodules at the corners and edges of the sample (Figure 9(b)) and the observance of the breakdown stage. The ability of the alloy to resist nodule formation was highly dependent upon aluminum content. The 15 and 20 wt pct Al samples did not develop nodule formations for any of the exposure times. However, as the aluminum content decreased, the time to nodule formation, or conversely, the length of inhibition stage, also decreased (Figure 15).

From the literature, there appears to be a lack of agreement concerning nodule nucleation and growth on Fe-based alloys.[32–37] Available mechanisms[32,33,34] for this type of growth in sulfur-containing environments are based primarily upon scale disruptions or mechanical failures in an initially formed passive layer that cannot re-establish itself. Therefore, the defect structure appears to be related to the growth and maintenance of the alumina scale and not the stoichiometry, or defect structure, of the alumina phase. This was easily observed by the growth of iron-sulfide platelets occurring in the alumina grain boundaries (Figure 7(b)) and not through the lattice of the scale itself. While the grain boundaries may be considered a "defect" in the scale, they did not appear to be deleterious to the integrity of the scale, as no sulfur was found to penetrate the alloy beneath these growths, and weight gains still remained negligible. Therefore, for growth of corrosion nodules to occur, a catastrophic event must take place in which the mechanical integrity of the alumina scale degrades and re-establishment cannot occur.

This ability of the initial oxide scale to re-establish itself was primarily related to the aluminum content of the alloy (Figure 15). As previously stated, formation of the alumina scale will deplete the alloy near the surface due to selective oxidation. Characteristics of this depletion region depend upon a number of factors including original alloy content, relative diffusivities in the alloy and scale, and exposure temperature. These three factors will dictate how quickly the aluminum is removed from the alloy, the extent of its depletion, and the ability to replenish or maintain the area with further additions of aluminum from the bulk. From the

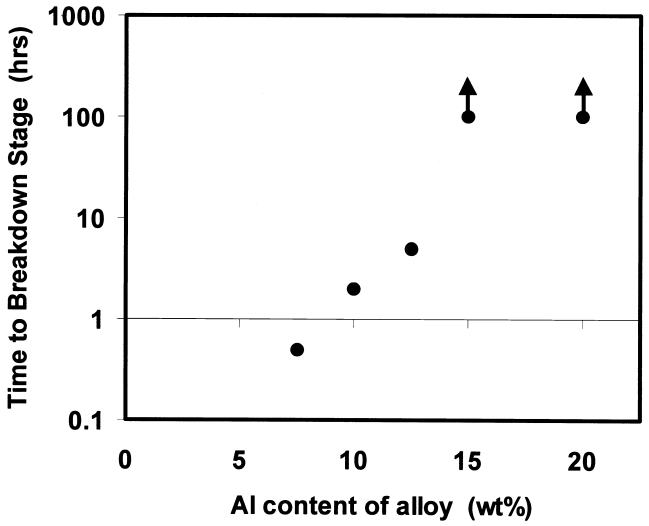

Fig. 15—The time to nodule formation, or breakdown stage, as a function of aluminum content. The *y*-axis is logarithmic and the arrows indicate that nodule formation did not occur up to 100 h of exposure.

preceding discussion, this will have a large bearing on the protective nature and oxidation lifetime of the alloy. When the alloy content was such that the amount of aluminum present at the alloy-scale interface remained relatively high, mechanical failures of the alumina scale were readily healed by reforming the scale in the fractured regions. Thus, the formation of gross sulfide phases, and the observance of the breakdown stage, was not seen for these alloys over the 100 hour exposure. An example of this is for the 15 and 20 wt pct Al alloys. These are iron aluminide (intermetallic) compositions and have typically exhibited very long oxidation lifetimes due to their large reservoirs of aluminum.[3,5–12,16,17]

When the content of aluminum at the alloy-scale interface was insufficient to ensure re-establishment of the original scale, growth of the fast-growing iron sulfide phases occurred in the fracture site due to an anion short circuiting mechanism by sulfur. This was primarily found on the 7.5 wt pct Al samples, and in some instances, on the 10 and 12.5 wt pct Al alloys. However, it is interesting to note that an aluminum depletion region was not observed beneath the oxide scale on any alloy after any exposure time within resolution limits of the equipment. Since diffusion in alumina scales is much slower than in the alloy and the rate of aluminum consumption, due to scale development, was very low, it could be expected that a depletion layer may not be found as Al from the bulk readily diffuses to the surface. Therefore, with mechanical failure of the scale, sulfur is now able to permeate the initial protective layer by means of a short circuiting mechanism or by direct contact with the substrate. The local equilibrium (in terms of $p(O_2)$ and $p(S_2)$) in the alloy beneath the scale has now changed from that previously observed at the gas-scale interface and fast growing sulfide phases were promoted. Therefore, it appears that the amount of aluminum present at the surface of the alloy, *e.g.*, the 7.5 wt pct Al samples, was initially high enough to form a protective scale but not to suppress formation of the sulfide phases below it upon scale fracture.

It is important to note here that while nodular formation on the alloys occurs by the same mechanism (mechanical

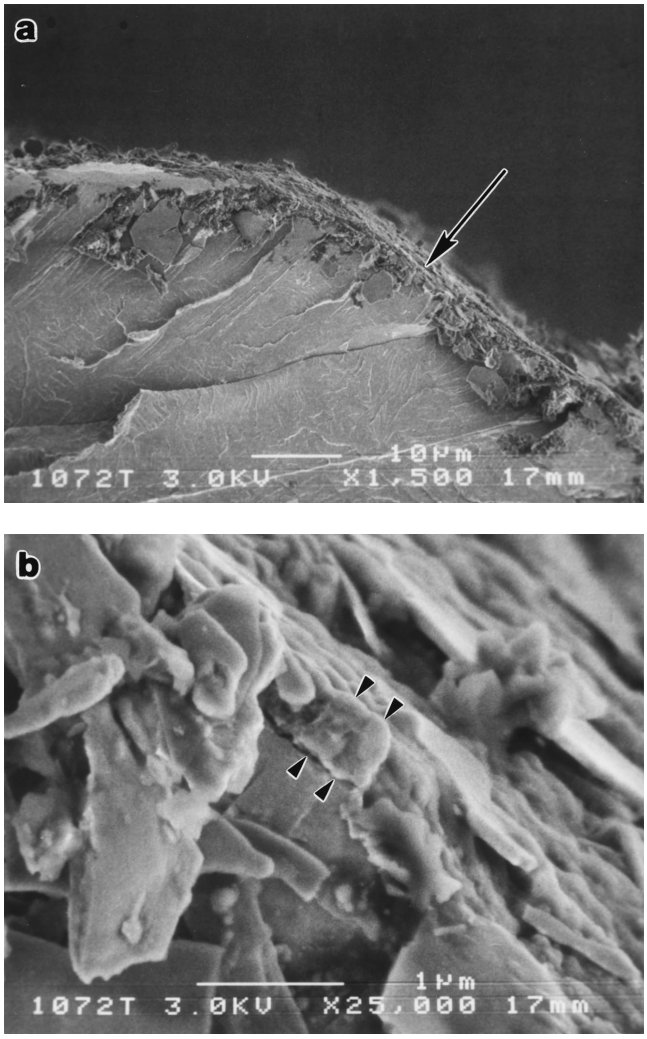

Fig. 16—(*a*) and (*b*) SE images of fractured cross section on the corner of the Fe-10 wt pct Al sample exposed at 700 °C for 50 h. Arrows indicate the scale thickness at approximately 700 nm.

failure and inability to re-establish the alumina scale), the reasons for the latter half of the mechanism may be different. As previously discussed, the 7.5 wt pct Al samples have nodules dispersed across their faces due to the inability to heal the mechanical disruption of the passive scale. This inability was related to the low aluminum content of the alloy. However, for the 10 and 12.5 wt pct Al samples, nodule growth also occurred at longer times (Figure 9(b)) but only in regions near the corners or edges of the specimen and did not appear on the flat faces of the sample. These areas located at the edges were found to grow thicker alumina scales (Figure 16) relative to the rest of the surface (Figure 7(c)) by nearly seven times. This may have lead to a higher depletion rate of aluminum and/or higher growth stresses in this area and further increase the probability of the scale failure or inability to re-establish itself upon breakdown. Other studies[37] have also found that the nodular growths tend to form at highly stressed areas of the specimen, such as corners and edges, or at regions of crystal misfit such as substrate grain boundaries or triple points; these areas typically allow for enhanced diffusion. Therefore, for the 10 and 12.5 wt pct Al alloys, it may be the sample geometry that led to the observance of the breakdown stage and not

the lack of protection afforded by the alloy. The growth of these few sulfide nodules on the 10 wt pct Al samples may account for the slightly higher weight gain attained, as seen in Figure 2.

Growth of the nodules was seen to occur by counterdiffusion of sulfur inward and iron outward, in combination with the continuous lateral degradation of the passive scale. The resulting morphologies were observed to be very complex as the corrosion product growth was no longer solely a uniform process of ion diffusion but contained an element of lateral growth across the surface as well. This was substantiated by the lenticular shape of the nodule in cross section, as well as by comparing the growth of the nodule diameters to the corrosion product penetration into the scale (Figure 11). Assuming that when the scale first breaks down, sulfur is initially allowed access to the underlying substrate in order to react at the alloy-scale interface. If growth of the nodules occurs exclusively through a diffusional process, then the lateral growth should be on the same order of magnitude as the perpendicular penetration. From the *n* values calculated and shown in Table III, this type of comparison cannot even be made as growth of the nodule diameter was linear ($n = 0.95$) and the inner scale development was near parabolic ($n = 0.63$). It can also be noted that as the sulfide products grew underneath the alumina scale, differences in phase volume caused expansion beneath the outer iron sulfide layer and the nodule was found to expand outward into the gas (Figure 12(a)), giving the nodule a lenticular appearance in cross section. This may place additional stresses within the protective scale and may lead to further failure with the nodules spreading until their eventual coalescence at long times.

3. *Steady-state stage*

As the aluminum content of the alloy was further decreased to 5 wt pct and below, the formation of alumina, and either of the first two corrosion stages, was never directly observed. Instead, thick scale growths (Figures 3 and 4) accompanied by relatively high weight gains (Figure 2) were observed, even at the shortest time. The growth of the outer iron sulfide layer for both the low carbon steel and Fe-Al sample occurred due to iron diffusion outward. Scale development began with nucleation and growth of randomly oriented iron sulfide grains on the surface. With the 5 wt pct Al sample, iron sulfide grains that were oriented in a favorable direction had preferential growth, which ultimately resulted in an outer layer of thick "columnar" grains (Figure 4(a)). However, where the low-carbon steel sample developed a relatively dense scale from the widespread growth and impingement of the iron sulfide plates at an early stage (Figure 3(a)), the scale on the 5 wt pct Al sample was found to be very porous from what appears to be a decreased number of favorably oriented grains that grew with time. Therefore, it appears that the addition of aluminum has resulted in a fewer number of favorably oriented iron-sulfide grains being able to grow, or conversely, that it has inhibited the other grains from growing. This may be related to the 1 wt pct of aluminum found in solution in the iron sulfide phase at the inner scale-outer scale interface (Table II). Strafford and Manifold[38] have observed slower diffusion rates of iron in iron sulfide due to the incorporation of aluminum (again, approximately 1 wt pct) in the scale during sulfidation experiments of Fe-Al alloys in this temperature range. Providing that the aluminum was substitutionally found in the iron sulfide, they surmised that creation of localized strain fields in the FeS lattice may have occurred due to the incorporation of the aluminum ions into the structure. These strain fields may act as sinks for cation vacancies and, hence, slow down the vacancy diffusion rate that in turn will reduce the cation diffusion rate outward.

Table IV. Calculated Parabolic Rate Constants for the Growth of the Outer Iron Sulfide Scales on the Low-Carbon Steel and Fe-5 Wt Pct Al Samples Using Cross-Sectional Scale Thicknesses

Alloy	Scale Measurement	k_p (cm^2/s)	Fit (R^2)
Low-carbon steel	outer iron sulfide scale	1.0×10^{-8}	0.99
Fe-5 wt pct Al	outer iron sulfide scale	2.5×10^{-9}	0.99

The growth of the tau plates was observed to penetrate the alloy, suggesting that sulfur diffused inward. As the inner scale was porous (due to iron diffusion outward), it is believed that sulfur was able to easily penetrate the scale and diffuse along the phase boundaries between the tau plates and the alloy for further development at the corrosion front. This was in agreement with *n*-value calculations from measured cross-sectional lengths that reside between 0.5 and 1, suggesting a mixture of diffusion and linear kinetics for the growth of the inner layer (Table III).

Aluminum was also found to diffuse, however, in a more local manner. This can be observed in the formation of iron-sulfide particles residing in between the tau plates. These particles were formed as aluminum diffused in order to create the aluminum-rich tau phase. As no depletion layer was observed at the alloy-scale interface, and the solubility of aluminum in the outer iron sulfide scale is limited (around 1 wt pct), the aluminum from the attacked matrix was constrained in the inner layer and located in the tau plates.

Even though the protective alumina scale was not observed to form, small additions of aluminum led to the development of slower growing reaction products when compared to the low carbon steel sample. This reduced the overall weight gain (Figure 2) and overall scale thickness (comparison of Figure 4(a) to Figure 3(a)). The slower growth of the scale was attributed to impeding iron diffusion outward through the developing layers, both inner and outer, that formed on the 5 wt pct Al sample. In terms of determining the reaction rates of the 5 wt pct Al alloy exposed at 700 °C *via* the thermogravimetric data, problems were encountered due to the assumptions underlying Wagner's law[39] of oxidation necessary for this type of analysis being violated; these being a single-diffusing specie through a dense, continuous, single-phase scale. As shown in Figure 4, two layers have developed from the diffusion of three different specie (Fe, Al, and S). Therefore, thickness measurements of the outer iron-sulfide scale were made (Figure 5), fit to a $t^{1/2}$ relationship, and parabolic rate constants determined and compared to the low carbon steel sample, as near parabolic kinetics were observed for both samples (Table III). It was found that aluminum additions decreased the outer FeS scale growth by over an order of magnitude (Table IV). Strafford and Manifold[38] also observed that the overall sulfidation rate of iron was an order of magnitude greater than that of a 5 wt pct Al alloy at 700 °C.

B. *Fe-Al Alloys as Weld Overlay Coatings*

In regards to the practical usage of Fe-Al alloys as sulfidation resistant, weld overlay claddings, the results from this work need to be carefully analyzed. It was shown that good corrosion resistance occurred for alloys with 10 wt pct Al and above, while good mechanical properties, in terms of their weldability, reside below this nominal value. Consequently, there does not appear to be an overlap in the desired characteristics. However, a number of factors must also be considered. (1) The exposure temperature for these experiments (700 °C) would be considered very aggressive from the standpoint of boiler conditions, which rarely reside above 600 °C. Previous work[40] has shown that lowering the reaction temperature to 600 °C in a similar gas composition decreased the rate of reaction and, hence, the degradation of the material, by nearly an order of magnitude. (2) Aluminum contents residing just below 10 wt pct Al (*i.e.*, 9.0 or 9.5 wt pct) were not investigated. These alloys have been found to be weldable[2] and with their higher nominal aluminum contents, when compared to 7.5 wt pct alloys, may allow for them to have similar corrosion resistance as to that found with compositions at 10 wt pct. Therefore, it may be concluded that alloys with Al compositions approaching 10 wt pct may encompass the properties of both good weldability characteristics and corrosion resistance and may be viable candidates for further evaluation for use as sulfidation resistant coatings at actual service temperatures.

V. CONCLUSIONS

The objective of the present study was to investigate the corrosion behavior of iron-aluminum alloys in reducing environments at 700 °C. From this work, the following conclusions were drawn.

1. The corrosion behavior of Fe-Al alloys in oxidizing/sulfidizing environments was directly related to the aluminum content of the alloy. For high aluminum compositions (10 to 20 wt pct Al), protection was afforded due to the development of a thin, continuous alumina scale that inhibited rapid degradation of the alloy. Increasing the aluminum content was found to promote the formation and maintenance of this scale. Alloy contents at or below 7.5 wt pct Al lead to high wastage rates from the formation of thick sulfide phases.

2. Three stages of corrosion behavior were observed by the Fe-Al alloys. The inhibition stage was characterized by relatively low weight gains due to the formation of a passive, thin alumina scale that offered protection. Localized mechanical failure of the alumina scale with subsequent growth of sulfide nodules resulted in the occurrence of the breakdown stage where the initially low weight gains were replaced by relatively high corrosion rates. The final stage observed was the near parabolic, steady-state growth of a continuous sulfide scale that relied upon diffusion through the previously formed product.

ACKNOWLEDGMENTS

This research was sponsored by the Fossil Energy Advanced Research and Technology Development (AR&TD) Materials Program, United States Department of Energy, under Contract No. DE-AC05-96OR22464 with Lockheed Martin Energy Research Corporation. The authors thank V.K. Sikka and P.F. Tortorelli, ORNL, for the cast Fe-Al alloys used in corrosion testing and technical discussions, respectively.

REFERENCES

1. K.R. Luer, J.N. DuPont, and A.R. Marder: *Corrosion*, 2000, vol. 56 (1), pp. 54-65.
2. S.W. Banovic, J.N. DuPont, and A.R. Marder: *Weld J.*, 1999, Jan., pp. 23s-30s.
3. J.H. DeVan: in *Oxidation of High-Temperature Materials*, T. Grobstein and J. Doychak, eds., TMS, Warrendale, PA, 1988, pp. 107-15.
4. C.G. McKamey, J.H. DeVan, P.F. Tortorelli, and V.K. Sikka: *J. Mater. Res.*, 1991, vol. 6 (8), pp. 1779-1805.
5. P.F. Tortorelli and J.H. DeVan: *Mater. Sci. Eng.*, 1992, vol. A135 (1–2), pp. 573-77.
6. J.H. DeVan and P.F. Tortorelli: *Corros. Sci.*, 1993, vol. 35 (5–8), pp. 1065-71.
7. P.F. Tortorelli, J.H. Devan, and U.K. Abdali: *Corrosion 93*, New Orleans, LA, 1993, paper no. 258.
8. J.H. DeVan and P.F. Tortorelli: *Mater. High Temp.*, 1993, vol. 11 (1–4), pp. 30-35.
9. P.F. Tortorelli and J.H. DeVan: *Processing, Properties, and Applications of Iron Aluminides*, TMS, Warrendale, PA, 1994, pp. 257-70.
10. K. Natesan and R.N. Johnson: in *Heat-Resistant Materials II*, K. Natesan, P. Ganesan, and G. Lai, eds., ASM INTERNATIONAL, Materials Park, OH, 1995, pp. 591-99.
11. P.F. Tortorelli, I.G. Wright, G.M. Goodwin, and M. Howell: *Elevated Temperature Coatings: Science and Technology II*, Anaheim, CA, Feb. 4–8, 1996, TMS, Warrendale, PA, 1996, pp. 175-86.
12. P.F. Tortorelli and K. Natesan: *Mater. Sci. Eng.*, 1998, vol. A285, pp. 115-25.
13. S.A. David, J.A. Horton, C.G. McKamey, T. Zacharia, and R.W. Reed: *Weld J.*, 1989, Sept., pp. 372s-381s.
14. P.J. Maziasz, G.M. Goodwin, C.T. Liu, and S.A. David: *Scripta Mater.*, 1992, vol. 27 (12), pp. 1835-40.
15. A.A. Fasching, D.I. Ash, G.R. Edwards, and S.A. David: *Scripta Mater.*, 1995, vol. 32 (3), pp. 389-94.
16. W. Kai and R.T. Huang: *Oxid. Met.*, 1997, vol. 48 (1–2), pp. 59-86.
17. W. Kai, J.P. Chu, R.T. Huang, and P.Y. Lee: *Mater. Sci. Eng.*, 1997, A239–A240, pp. 859-70.
18. S.F. Chou, P.L. Daniel, A.J. Blazewicz, and R.F. Dudek: Report No. RDTPA 84-12, Babcock & Wilcox, Detroit, MI, Sept. 1984.
19. J.E. Gabrielson and E.D. Kramer: *1996 Int. Joint Power Generation Conf., Vol 1*, ASME, Fairfield, NJ, 1996, EC-vol. 4/FACT-vol. 21, pp. 19-23.
20. J.A. Urich and E. Kramer: *1996 Int. Joint Power Generation Conf., Vol 1*, ASME, Fairfield, NJ, 1996, EC-vol. 4/FACT-vol. 21, pp. 25-29.
21. *HSC Chemistry for Windows*, ver. 3.0, Outokumpu Research Oy, Pori, Finland, 1997, www.outokumpu.fi/hsc.
22. S.W. Banovic, J.N. DuPont, and A.R. Marder: Lehigh University, Bethlehem, PA, unpublished research, 1988.
23. J.I. Goldstein, D.E. Newbury, P. Echlin, D.C. Joy. A.D. Romig, Jr., C.E. Lyman, C. Fiori, and E. Lifshin: *Scanning Electron Microscopy and X-ray Microanalysis*, 2nd ed., Plenum Press, New York, NY, 1992.
24. W.C. Hagel: *Corrosion*, 1965, vol. 21, pp. 316-26.
25. R. Prescott and M.J. Graham: *Oxid. Met.*, 1992, vol. 38 (3–4), pp. 233-54.
26. H. Hindam and D.P. Whittle: *Oxid. Met.*, 1982, vol. 18 (5–6), pp. 245-84.
27. K.N. Strafford and P.K. Datta: *Corros. Sci.*, 1993, vol. 35 (5–8), pp. 1053-63.
28. B.A. Pint: in *Fundamental Aspects of High Temperature Corrosion*, D.A. Shores, R.A. Rapp, and P.Y. Hou, eds., Electrochemical Society, Pennington, NJ, 1997, pp. 74-85.
29. W.J. Quaddakers and K. Bongartz: *Werjst. Korros.*, 1994, vol. 45, pp. 232-38.
30. W.J. Quaddakers and M.J. Bennett: *Mater. Sci. Technol.*, 1994, vol. 10, pp. 126-31.
31. R. Prescott and M.J. Graham: *Oxid. Met.*, 1992, vol. 38 (1–2), pp. 73-87.
32. W.E. Boggs: *J. Electrosc. Soc.*, 1971, vol. 118 (6), pp. 906-12.
33. P.C. Patnaik and W.W. Smeltzer: *Oxid. Met.*, 1985, vol. 23 (1–2), pp. 53-75.
34. N.S. Quan and D.J. Young: *Oxid Met.*, 1986, vol. 25 (1–2), pp. 107-19.

35. M. Sakiyama, P. Tomsazewski, and G.R. Wallwork: *Oxid. Met.*, 1979, vol. 13 (4), pp. 311-30.
36. P.J. Smith, R.M. Beauprie, W.W. Smeltzer, D.V. Stevanovic, and D.A. Thompson: *Oxid Met.*, 1987, vol. 28 (5–6), pp. 259-76.
37. P. Tomaszewicz and G.R. Wallwork: *Oxid. Met.*, 1983, 19 (5–6), pp. 165-85.
38. K.N. Strafford and R. Manifold: *Oxid Met.*, 1969, vol. 1 (2), pp. 221-40.
39. P. Kofstad: *High Temperature Corrosion*, Elsevier Applied Science Publishers Ltd., New York, NY, 1988, p. 19.
40. S.W. Banovic, J.N. DuPont, and A.R. Marder: in *Surface Engineering in Materials Science I*, S. Seal, N.B. Dahotre, J.J. Moore, and B. Mishra, eds., TMS, Warrendale, PA, 2000, pp. 301-10.